Physics

Physics Research Publications

Purdue University   *Year* 2005

Ground- and excited-state electronic structure of an iron-containing molecular spin photoswitch

J. H. Rodriguez

Ground- and excited-state electronic structure of an iron-containing molecular spin photoswitch

Jorge H. Rodriguez[a)]

Department of Physics, Purdue University, West Lafayette, Indiana 47907-2036

The electronic structure of the cation of $[Fe(ptz)_6](BF_4)_2$, a prototype of a class of complexes that display light-induced excited-state spin trapping (LIESST), has been investigated by time-independent and time-dependent density-functional theories. The density of states of the singlet ground state reveals that the highest occupied orbitals are metal centered and give rise to a low spin configuration $Fe^{2+}(3d_{xy}^{\uparrow\downarrow}3d_{xz}^{\uparrow\downarrow}3d_{yz}^{\uparrow\downarrow})$ in agreement with experiment. Upon excitation with light in the 2.3–3.3 eV range, metal-centered spin-allowed but parity-forbidden ligand field (LF) antibonding states are populated which, in conjunction with electron-phonon coupling, explain the experimental absorption intensities. The computed excitation energies are in excellent agreement with experiment. Contrary to simpler models we show that the LF absorption bands, which are important for LIESST, do not originate in transitions from the ground to a single excited state but from transitions to manifolds of nearly degenerate excited singlets. Consistent with crystallography, population of the LF states promotes a drastic dilation of the ligand cage surrounding the iron. © *2005 American Institute of Physics.* [DOI: 10.1063/1.2018631]

I. INTRODUCTION

Some iron-containing complexes have been found to exhibit optically and thermally induced spin crossovers whereby a transition is made from their singlet ground state to a long-lived (order of days) metastable high spin state.[1,2] In particular, upon excitation with green light, crystalline (Fig. 1) and powder forms of $[Fe(ptz)_6](BF_4)_2$ make spin-forbidden transitions from the low spin (LS) $S=0$ state to a high spin (HS) $S=2$ metastable state which becomes trapped below a critical temperature of about 50 K. This phenomenon is known as light-induced excited-state spin trapping (LIESST).[1] Such spin transitions are also observed upon thermal excitation at about 135 K and are accompanied by dramatic structural rearrangements whereby a rombohedral $\rightarrow$ triclinic phase transition also occurs.[3,4] Concomitant with the magnetic transitions are significant rearrangements of orbital occupation and spin configuration of the central Fe^{2+} valence shell which, in a cubic ligand field, can be described as $d_{xy}^{\uparrow\downarrow}d_{xz}^{\uparrow\downarrow}d_{yz}^{\uparrow\downarrow}d_{x^2-y^2}d_{z^2} \rightarrow d_{xy}^{\uparrow\downarrow}d_{xz}^{\uparrow}d_{yz}^{\uparrow}d_{x^2-y^2}^{\uparrow}d_{z^2}^{\uparrow}$. Similarly, the structural transitions are associated with unusually large Fe–N bond elongations of about 0.2 Å.[3,4]

Due to the ability to control spin transitions and color changes in $[Fe(ptz)_6](BF_4)_2$ by means of optical excitation, this and similar complexes are seen as photoswitches for potential use in novel molecular-level memory storage or liquid-crystal display applications.[2,5] Some progress has been made in understanding the basic mechanism of LIESST, mostly based on optical and other spectroscopies.[1,2,6] The qualitative mechanism for high spin trapping in $[Fe(ptz)_6] \times (BF_4)_2$ has been described as an excitation from the singlet ground state to other short-lived, higher-energy singlets (Fig. 2). This is followed by spin-forbidden intersystem crossing to an intermediate lower-energy triplet which, mediated by spin-orbit coupling, changes the total spin of the system by one unit. Another spin-forbidden intersystem crossing brings the system to the metastable quintet state where it is subsequently trapped below its critical temperature.[1,2,6]

Most of the optical experiments have focused on excitations of the initial $S=0$ and final $S=2$ states of LIESST complexes because these states can be trapped by controlling the temperature and their crystallographic structures have also been determined.[2–4,6] However, further theoretical understanding is needed about the detailed electronic structure of LIESST-exhibiting complexes. In particular; one wishes to elucidate their ground- and excited-state electronic structures, the origin of the optical absorption associated with the vertical singlet excited states, and how the excited-state electronic structures are related to the dramatic geometric changes observed by crystallography.[3,4] Such understanding will likely lead to the design and synthesis of new LIESST materials with higher critical temperatures (below which the high spin state is effectively trapped) for use in potentially novel memory storage or display technologies.[1,2,6] In this work, after a brief description of the ground-state electronic structure, we focus on the computation of singlet$\rightarrow$singlet excited states of the spin photoswitch $[Fe(ptz)_6](BF_4)_2$ by means of time-dependent density-functional response theory.[7–10]

II. THEORETICAL BACKGROUND

Kohn-Sham density-functional theory[11–13] (KS-DFT) yields the ground-state density $\rho^{KS}(\mathbf{r})=\Sigma_j^{N=occ}|\psi_j^{KS}(\mathbf{r})|^2$ and other ground-state properties of an N-electron system based on the solution of the Kohn-Sham equations which yield the

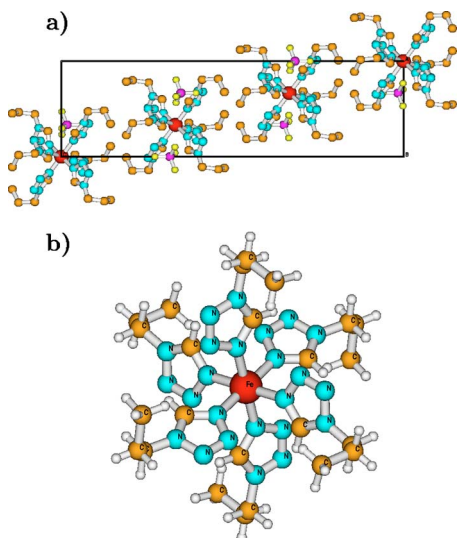[a)]Electronic mail: jorge-r@physics.purdue.edu

FIG. 1. (Color online) Crystallographic structure of $[Fe(ptz)_6](BF_4)_2$ (ptz=1-propyltetrazole) (Ref. 4): (a) Projection along the hexagonal b axis of a complete cell showing some of the Fe and counterion molecules with centers at zero height. (b) Structure of a single $[Fe(ptz)_6]^{2+}$ cation.

FIG. 2. Basic mechanism of light-induced excited-state spin trapping in $[Fe(ptz)_6](BF_4)_2$. Interaction of the $S=0$ multielectronic ground state with light promotes singlet→singlet vertical excitations to manifolds of either ligand field (LF) or metal to ligand charge-transfer (MLCT) states which are represented by arrows. The dashed lines represent radiationless spin-forbidden intersystem crossings to an intermediate triplet ($S=1$) and to a metastable quintet ($S=2$) state.

time-independent orbitals $\psi_j^{KS}(\mathbf{r})$. By contrast, time-dependent density-functional response theory[8–10] (TD-DFRT) provides a rigorous framework for the computation of excited-state properties and can be applied to finite systems such as single molecules. In particular, TD-DFRT can predict fairly accurate[14] excitation energies, oscillator strengths, and dipole moments associated with transitions from ground to excited states upon interaction of the system's electronic density with a resonant time-dependent electric perturbation. An starting point of TD-DFRT are the time-dependent Kohn-Sham equations which are expressed in terms of an effective potential for a noninteracting system of N electrons, $v_{eff}(\mathbf{r},t)$, that explicitly includes a time-dependent perturbation $v(\mathbf{r},t)$ and whose orbitals $\psi_j(\mathbf{r},t)$ yield the dynamic electron density $\rho(\mathbf{r},t)$ of the truly interacting system,[7,15]

$$\left[-\frac{1}{2}\nabla^2 + v_{eff}[\rho](\mathbf{r},t) \right]\psi_j(\mathbf{r},t) = i\frac{\partial}{\partial t}\psi_j(\mathbf{r},t), \quad (1)$$

where $\rho(\mathbf{r},t) = \Sigma_j^N |\psi_j(\mathbf{r},t)|^2$ and the effective potential is given by

$$v_{eff}[\rho](\mathbf{r},t) = v(\mathbf{r},t) + \int \frac{\rho(\mathbf{r},t)}{|\mathbf{r}-\mathbf{r}'|}d\mathbf{r}' + v_{xc}[\rho](\mathbf{r},t). \quad (2)$$

In (2) the exchange-correlation potential accounts for the nonclassical interactions and corresponds to the functional derivative of the exchange-correlation action which, within the adiabatic approximation, is approximated as the exchange-correlation energy of time-independent Kohn-Sham theory[11–13] evaluated at a particular t:

$$v_{xc}[\rho](\mathbf{r},t) = \frac{\delta A_{xc}[\rho(\mathbf{r},t)]}{\delta\rho(\mathbf{r},t)} \approx \frac{\delta E_{xc}[\rho^t(\mathbf{r})]}{\delta\rho^t(\mathbf{r})} = v_{xc}[\rho^v](\mathbf{r}). \quad (3)$$

For the computation of polarizabilities, excitation energies, and oscillator strengths only the linear response of the den-
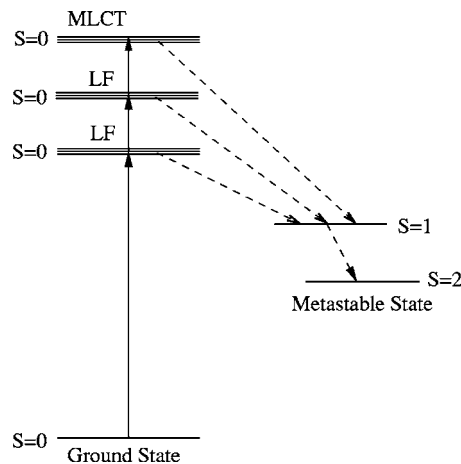
sity is needed which allows for a perturbative solution to the time-dependent Kohn-Sham equations. The average frequency-dependent dynamic polarizability $\bar{\alpha}(w)$ describes the response of the system's dipole moment to a weak time-dependent electric field (perturbation) and can be evaluated from the linear response of the time-dependent electron density. This in turn allows the computation of excited-state energies in the frequency domain w_i and corresponding oscillator strengths f_i, which are shown as poles and residues, respectively, in the sum-over-states expression for the dynamic polarizability:[8–10]

$$\bar{\alpha}(-w;w) = \sum_i \frac{f_i}{w_i^2 - w^2} = \frac{2}{3}\sum_i \frac{w_i\mu_i^2}{w_i^2 - w^2}. \quad (4)$$

In (4) only the dipole-allowed transitions contribute to the summation,[16] $w_i \equiv E_i - E_o$ are the vertical excitation frequencies, $-w$ corresponds to the sum of these frequencies, and μ_i^2 are the squared magnitudes of the transition dipole moments.[8–10] Herein, we report on the ground- and excited-state properties of the cation of $[Fe(ptz)_6](BF_4)_2$ based on time-independent and time-dependent density-functional calculations, respectively.

The Kohn-Sham orbitals which yield the ground-state electron density and have energies ϵ_j are expanded in terms of atom-centered basis functions $\chi_\mu(\mathbf{r})$, which mimic atomic orbitals $\psi_j^{KS}(\mathbf{r}) = \Sigma_\mu c_{\mu j}\chi_\mu(\mathbf{r})$. Analysis of the composition of individual molecular orbitals allows the computation of partial density of states (PDOS) contributions from individual atom-centered basis to the total density of states (TDOS). In particular, the partial contribution to the DOS from a basis function χ_μ can be expressed as $PDOS_\mu(E) = \Sigma_j\Sigma_\nu c_{\mu j}c_{\nu j}\langle\chi_\nu|\chi_\mu\rangle\delta(E-\epsilon_j)$ where one substitutes the delta function by broadened Gaussians.[17]
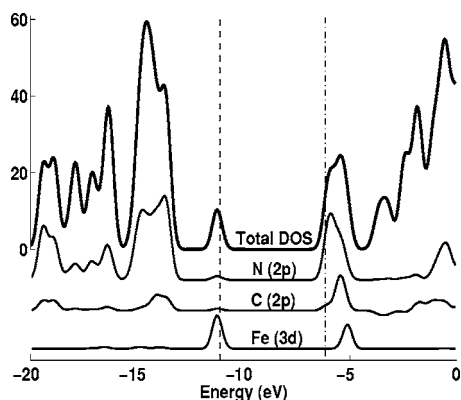
FIG. 3. Total and partial density of states (DOS) around the HOMO-LUMO gap for the multielectronic singlet ground state ^1A_g of $[Fe(ptz)_6]^{2+}$. The partial DOSs corresponding to contributions of valence shells from the iron ion or tetrazole (Tz) fragments are also shown: Fe($3d$), Tz N($2p$), and Tz C($2p$). The dashed vertical lines indicate energies of the HOMO:MO 192 (left) and LUMO: MO 193 (right), respectively. Ground-state DFT calculations used the B3LYP functional (Refs. 18–20) and the all-electron basis 6-311G(d,p) (Ref. 29) as implemented in GAUSSIAN 98 (Ref. 23).

III. RESULTS AND DISCUSSION

The ground-state electronic structure of $[Fe(ptz)_6]^{2+}$ can be conveniently interpreted in terms of DOS plots as shown in Fig. 3 where the left and right dashed lines correspond to the highest occupied molecular orbital (HOMO) and lowest unoccupied molecular orbital (LUMO) energies, respectively. The partial DOS reveal that the HOMOs are fairly localized on the metal ion with only minor, but nonzero, contributions from nitrogens and carbons of the tetrazole (Tz) rings. By contrast, the lowest unoccupied orbitals (MO 193–204) are highly delocalized throughout the tetrazole rings with almost negligible contributions from Fe-centered orbitals. The localized or delocalized behavior of some representative orbitals is shown in Figs. 4 and 5. In particular, the localized HOMO (MO 192) and delocalized LUMO (MO
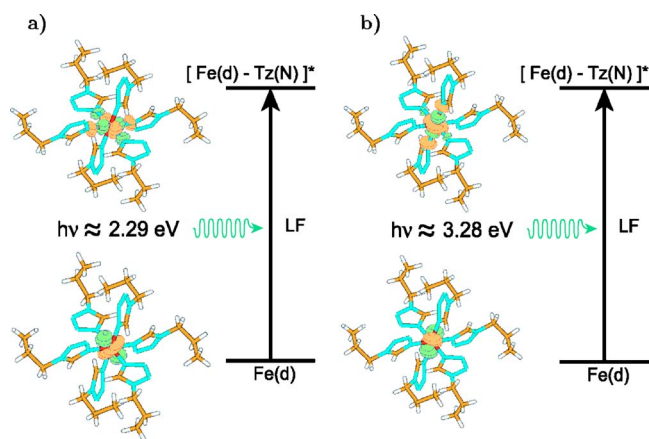

FIG. 4. (Color online) (a) The dominant contribution to the lowest-energy transition shown in Table I: excited state 1 of ligand field (LF) character. An electron excitation occurs from iron-centered MO 192 (HOMO) to unoccupied MO 206 which is mainly an Fe($3d$) orbital antibonding with N($2p$) orbitals of four neighboring tetrazole nitrogens. (b) One of the dominant contributions to the lower-energy transitions shown in Table I: excited states 1, 3, and 5 of ligand field (LF) character. An electron excitation from iron-centered MO 191 to unoccupied MO 205 which is mainly an Fe($3d$) orbital antibonding with N($2p$) orbitals of two neighboring tetrazole nitrogens.
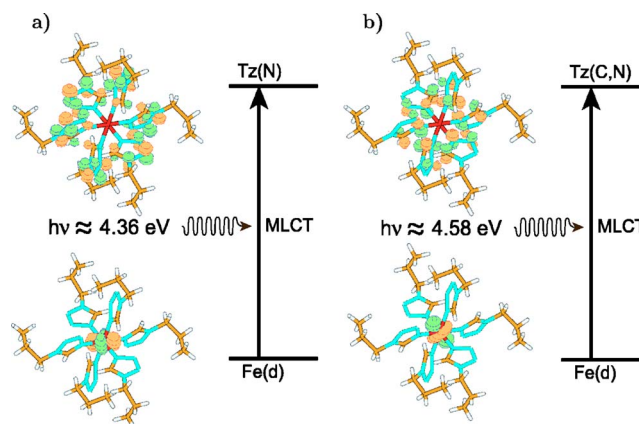

FIG. 5. (Color online) (a) The dominant contribution to a formally allowed MLCT transition (excited state 13, $f=0.0078$). An electron excitation occurs from iron-centered MO 190 to unoccupied MO 193 (LUMO) which is delocalized throughout the tetrazole rings. (b) The dominant contributions to the MLCT transition with largest oscillator strength (excited state 23, $f=0.1435$). An excitation occurs from iron-centered MO 192 (HOMO) to unoccupied MO 199 which is delocalized throughout Tz(C,N) orbitals.

193) are shown in Figs. 4(a) and 5(a), respectively. Slightly above the LUMO energy, however, some orbitals (MO 205 and 206) have main Fe($3d$) character with non-negligible contributions from tetrazole rings which are antibonding to the metal [Figs. 4(a) and 4(b)]. We notice that this particular ordering of the unoccupied frontier orbitals (LUMOs) is somewhat dependent on the chosen exchange-correlation functional (B3LYP) (Refs. 18–20) which is here used to describe ground- and excited-state electronic structures. The use of an alternative functional (BPW91) (Refs. 21 and 22) yielded a somewhat differing ordering whereby the lowest-energy LUMOs are metal based and those slightly higher in energy are tetrazole based. However, as described below, the basic qualitative description of the excited-state properties via TD-DFRT is the same for both types of representative functionals. To confirm the results, ground-state calculations were carried out for C_i and S_6 symmetries with two representative electronic structure packages (GAUSSIAN 98:[23] B3LYP/6-311G* and JAGUAR 4.2:[24] B3LYP/LACVP**). The qualitative results obtained from both packages were identical. Excited-state calculations were done within the C_i group with GAUSSIAN 98.[23]

The ground-state properties described above provide a useful reference for understanding the excited states of the complex within the framework of TD-DFRT.[8–10] Here, excited states are expanded in terms of several single-electron excitations from particular occupied to particular unoccupied Kohn-Sham orbitals as shown in Table I. All the low-energy transitions with finite oscillator strength involve excitations from Kohn-Sham orbitals of even symmetry to those of odd symmetry ($g \rightarrow u$). This is true for orbitals obtained from ground-state calculations within the C_i and S_6 symmetry groups and whose respective labels are given in Table II. In particular, the lowest-energy excited state with finite oscillator strength (excited state 7) corresponds to a transition from the HOMO (MO 192) with symmetry label A_g to the LUMO (MO 193) with label A_u (Tables I and II). The basic qualitative description of the excitations with finite oscillator

TABLE I. Properties of selected vertical singlet excited states of $[Fe(ptz)_6]^{2+}$ obtained from TD-DFRT. Calculations used the B3LYP functional and the all-electron basis 6-31G* as implemented in GAUSSIAN 98 (Ref. 23).

Excited state	C_i label	E (eV)	f^a	$\psi_{occ}^{KS} \rightarrow \psi_{unocc}^{KS}$ [b]	Dominant	character[c]
1	^1A_g	2.291	0.0000[a]	$192 \rightarrow 206$	$Fe \rightarrow (Fe-N)$	
				$192 \rightarrow 205$	$Fe \rightarrow (Fe-N)$	
				$191 \rightarrow 205$	$Fe \rightarrow (Fe-N)$	
				$190 \rightarrow 206$	$Fe \rightarrow (Fe-N)$	
2	^1A_g	2.291	0.0000[a]	$192 \rightarrow 205$	$Fe \rightarrow (Fe-N)$	
				$192 \rightarrow 206$	$Fe \rightarrow (Fe-N)$	
				$190 \rightarrow 205$	$Fe \rightarrow (Fe-N)$	
				$191 \rightarrow 206$	$Fe \rightarrow (Fe-N)$	
3	^1A_g	2.346	0.0000[a]	$190 \rightarrow 206$	$Fe \rightarrow (Fe-N)$	
				$191 \rightarrow 205$	$Fe \rightarrow (Fe-N)$	
4	^1A_g	3.277	0.0000[a]	$192 \rightarrow 205$	$Fe \rightarrow (Fe-N)$	
				$190 \rightarrow 205$	$Fe \rightarrow (Fe-N)$	
				$191 \rightarrow 206$	$Fe \rightarrow (Fe-N)$	
5	^1A_g	3.277	0.0000[a]	$192 \rightarrow 206$	$Fe \rightarrow (Fe-N)$	
				$190 \rightarrow 206$	$Fe \rightarrow (Fe-N)$	
				$191 \rightarrow 205$	$Fe \rightarrow (Fe-N)$	
6	^1A_g	3.317	0.0000[a]	$191 \rightarrow 206$	$Fe \rightarrow (Fe-N)$	
				$190 \rightarrow 205$	$Fe \rightarrow (Fe-N)$	
7	^1A_u	4.178	0.0003	$192 \rightarrow 193$	$Fe \rightarrow Tz(N)$	
10	^1A_u	4.331	0.0206	$192 \rightarrow 196$	$Fe \rightarrow Tz(N)$	
11	^1A_u	4.331	0.0206	$192 \rightarrow 197$	$Fe \rightarrow Tz(N)$	
12	^1A_u	4.358	0.0077	$191 \rightarrow 193$	$Fe \rightarrow Tz(N)$	
13	^1A_u	4.358	0.0078	$190 \rightarrow 193$	$Fe \rightarrow Tz(N)$	
18	^1A_u	4.462	0.0001	$190 \rightarrow 196$	$Fe \rightarrow Tz(N)$	
				$191 \rightarrow 197$	$Fe \rightarrow Tz(N)$	
19	^1A_u	4.498	0.0001	$192 \rightarrow 199$	$Fe \rightarrow Tz(C,N)$	
				$190 \rightarrow 196$	$Fe \rightarrow Tz(N)$	
20	^1A_u	4.499	0.0168	$191 \rightarrow 197$	$Fe \rightarrow Tz(N)$	
				$190 \rightarrow 196$	$Fe \rightarrow Tz(N)$	
21	^1A_u	4.499	0.0167	$190 \rightarrow 197$	$Fe \rightarrow Tz(N)$	
				$191 \rightarrow 196$	$Fe \rightarrow Tz(N)$	
23	^1A_u	4.582	0.1435	$192 \rightarrow 199$	$Fe \rightarrow Tz(C,N)$	

[a]Values obtained for C_i symmetry. A minor change of a single Fe–N bond lowers the symmetry to C_1 which makes the formally zero oscillator strengths to acquire small values ($10^{-3} - 10^{-4}$).

[b]Only the dominant single-electron excitations which contribute to a particular excited state are shown in order of importance. Some excited states have several dominant such contributions and others, e.g., excited state 7, have only one.

[c](Fe–N) indicates unoccupied antibonding MOs with a dominant Fe(3d) contribution which is antisymmetric to a minor contribution from neighboring N(p) orbitals. Tz(N) or Tz(C) indicate unoccupied MOs with dominant tetrazole N(p) or tetrazole C(p) contribution, respectively.

strength is the same for B3LYP (Refs. 18–20) and BPW91 (Refs. 21 and 22) (not shown) functionals even though the relative ordering of their unoccupied Kohn-Sham orbitals is somewhat different. Thus, for both functionals, the lowest-energy excited state with formally finite oscillator strength mainly corresponds to a HOMO(MO 192, A_g) $\rightarrow$ LUMO(MO 193, A_u) transition.

Although single-crystal absorption spectra of $[Fe(ptz)_6]$ $\times (BF_4)_2$ display rather broad and unresolved bands around 2.28 eV ($\approx 18\,400$ cm^{-1}) and 3.30 eV ($\approx 26\,650$ cm^{-1}),[1] contrary to simpler models,[1,2,6] the time-dependent calcula-

tions revealed that each of these bands is a complex superposition of several singlet$\rightarrow$singlet excitations which are closely packed on the energy scale. The computed excitation energies are given in Table I and very closely agree with the experimental values. In particular, excited states 1 and 2 where calculated at 2.29 eV with respect to the ground state in remarkable agreement with the measured energy of the first absorption band around 2.28 eV.[1] Similarly, excited states 4 and 5 were calculated at 3.28 eV above the ground state in close agreement with the measured value for the second band around 3.30 eV.[1] Recent TD-DFRT calculations

TABLE II. Labels of relevant ground-state Kohn-Sham orbitals for C_i and S_6 symmetry groups.

ψ^{KS}	Type	C_i	S_6
190	Occupied	A_g	E_g
191	Occupied	A_g	E_g
192	Occupied	A_g	A_g
193	Unoccupied	A_u	A_u
196	Unoccupied	A_u	E_u
197	Unoccupied	A_u	E_u
199	Unoccupied	A_u	A_u
205	Unoccupied	A_g	E_g
206	Unoccupied	A_g	E_g

have also shown close agreement with experiment for a related iron complex.[14] Computed excited states 1–3 and 4–6 (Table I) are, therefore, identified with the 2.28 and 3.30 eV absorption bands of the experimental spectrum, respectively. Furthermore, the TD-DFRT calculations show that these bands do not correspond to excitations from the ground to a single excited state but that each of these is a superposition of nonresolved intensities corresponding to some three excited states which are close on the energy scale. These six lower-energy transitions 1–3 and 4–6, have main ligand field (LF), Fe$(3d) \rightarrow$ Fe$(3d)$, character as illustrated by Figs. 4(a) and 4(b) whereby metallic electron density is transferred to higher-energy states dominated by antisymmetric (antibonding) combinations of Fe$(3d)$ orbitals and small contributions from tetrazole nitrogen orbitals. The substantial ligand field (LF) character predicted for these transitions is also consistent with their lower intensities and lower energies in the experimental spectrum relative to those measured around 4.18–4.58 eV which, as described below, are clearly of metal to ligand character and, therefore, expected to be more intense and higher in energy. Table I shows the computed energies and other properties of the most relevant singlet $\rightarrow$ singlet excitations. The crystallographic structure of a single molecular complex very closely corresponds to S_6 symmetry with the largest Abelian subgroup being C_i in which the iron is the center of inversion. The C_i molecular symmetry used in the KS-DFT and TD-DFRT calculations gave rise to a ^1A_g multielectronic ground state which formally does not produce finite transition dipole moments with the lower-energy excited states of the same symmetry. For centrosymmetric molecules with inversion symmetry, transitions of equal parity $(g \rightarrow g)$ are formally forbidden whereas those of different parity $(g \rightarrow u)$ are allowed. Accordingly, the six lowest-energy transitions (i.e., excited states 1–6) yielded a formally zero oscillator strength $(f=0)$ which, however, became finite upon lowering the molecular symmetry to C_1. In fact, shortening one of the Fe–N bonds by ≈ 0.1 Å introduced a slight distortion which produced small but finite oscillator strengths $(f \approx 10^{-3}$–$10^{-4})$ for excitation energies around 2.3–3.3 eV corresponding to excited states 1–6. We are further studying the origin of the finite LF intensities observed in the experimental spectrum. However, comparison of our TD-DFRT calculations performed with C_i and C_1 symmetry strongly suggests that the lower-energy LF bands originate from meaningful distortions from the nomi-

nal C_i symmetry. It is known that formally forbidden $g \rightarrow g$ transitions can become allowed if the center of symmetry is eliminated during asymmetric vibrations. Thus, the distortions from the nominal symmetry most likely originate in the coupling of electronic and nuclear degrees of freedom (vibronic coupling) which has been shown to yield sizable absorption intensities for otherwise parity-forbidden transitions within the context of TD-DFRT.[25] Other studies on related LIESST crystals have also shown that coupling of the electronic state and the phonon system plays a dominant role on their phase transitions.[26,27] In addition, crystal packing forces may lower the molecular symmetry relative to the gas-phase calculations reported here further promoting absorption intensity.

For C_i symmetry all the lower-energy transitions with formally finite oscillator strength (excited states 7, 10, 11,…, Table I) clearly correspond to singlet $\rightarrow$ singlet metal to ligand charge transfers (MLCT). Some representative examples are shown in Figs. 5(a) and 5(b). Most of these nearly degenerate excited states had a dominant Fe$(3d) \rightarrow$ Tz(N) character whereby metal-centered electron density was mainly transferred to the nitrogens of the tetrazole rings. The most intense MLCT transition (excited state 23, $f=0.1435$), however, corresponds to transfer of metallic electron density to an excited state of dominant Tz(C,N) character. By lowering the molecular symmetry to C_1 these metal to ligand excitations also produced a somewhat greater oscillator strength. The experimental spectrum recorded at 8 K shows that the two lower-energy LF bands have extinction coefficients of $\gtrsim 20$ 1/mol cm and $\lesssim 30$ 1/mol cm, respectively, whereas that of the MLCT band is presumably much larger since it falls outside the range of the published data.[1,6] This is qualitatively consistent with the small oscillator strength we estimate (Table I) for the LF bands within C_1 symmetry ($f = 10^{-3}$–10^{-4}) and with the substantially higher oscillator computed for the most intense MLCT excitation (excited state 23, $f=0.1435$).

The excited-state properties determined from the present TD-DFRT calculations provide insight on the initial mechanisms of light-induced excited-state spin trapping (LIESST). The lower-energy absorption bands observed experimentally around 2.28 and 3.30 eV originate in ligand field (LF) transitions which transfer electron density from localized Fe$(3d)$ orbitals to antibonding states of main Fe$(3d)$ character with additional Tz(N) contributions: Fe$(3d) \rightarrow [$Fe$(3d) -$Tz:N$(2s,2p)]^*$. As shown in Figs. 4(a) and 4(b), the minor Tz(N) contributions to these antibonding states are localized on the nitrogens which are chemically bound to the iron. The antibonding nature of the metal-ligand interactions in these excited states in turn weakens the Fe–N bonds and promotes their elongation. Although the crystallographic structures of the ground singlet and metastable quintet states of $[$Fe(ptz)$_6](BF_4)_2$ show dramatic structural rearrangements and Fe–N bond lengths which are about 0.2 Å longer for the latter state, no clear microscopic understanding exists about the origin of such elongations. The present results show that electromagnetic absorption close to the green region (2.28–3.30 eV) is inherently associated with the formation of vertical antibonding excited states which promote elonga-

tion of the Fe–N bonds. This follows since to reach equilibrium in the excited state the nuclear coordinates must, in general, relax. Therefore, the structural rearrangements crystallographically detected for the metastable quintet likely begin to appear before this state is actually formed, namely, at the beginning stages of the LIESST process when the antibonding singlets are formed and, thereafter, at the initial (singlet-triplet) intersystem crossing. This is consistent with recent spectroscopic studies suggesting that the ligand field $Fe(3d) \rightarrow Fe(3d)$ transitions more efficiently drive the cooperative change in spin state than other excitation bands[27] and also with our own geometry optimizations for the intermediate triplet state which show longer Fe–N bonds relative to the ground-state singlet.[28]

IV. CONCLUSION

We have obtained the first detailed microscopic description of the ground- and excited-state electronic structures of the cation of the LIESST-exhibiting $[Fe(ptz)_6](BF_4)_2$ spin photoswitch. The complex is a prototype of a wider class of spin-forbidden crossover compounds and the qualitative insight gained here should apply to other such systems. Although there have been many experimental studies on the ground and metastable states of the complex, only limited theoretical information existed about the properties of its excited states. The present time-dependent calculations on the complete cationic molecular structure have provided a detailed microscopic description of the vertical singlet $\rightarrow$ singlet excitations which are observed in the experimental spectrum. The energies of the LF and higher-energy MLCT excitations have been calculated with remarkable accuracy relative to the experimental spectra. The essentially centrosymmetric crystalline structure of the cationic complex formally produces no or very weak ligand field $Fe(3d) \rightarrow Fe(3d)$ absorption intensities of strict electronic origin. Therefore, the formally parity-forbidden lower-energy LF bands mainly arise from vibronic transitions due to coupling of the electronic and phonon systems. Furthermore, such LF bands are not simple singlet $\rightarrow$ singlet excitations but arise from ground-state transitions to two manifolds of nearly degenerate excited states (1–3 and 4–6). Finally, the antibonding nature of the singlet LF excited states naturally promotes Fe–N bond elongations which strongly suggest that the dilation of the ligand cage surrounding the iron at the metastable quintet likely begins to appear at the onset of the LS $\rightarrow$ HS transition process, namely, at the optically or thermally induced occupation of the singlet antibonding states.

[1] S. Decurtins, P. Gutlich, K. M. Hasselbach, A. Hauser, and H. Spiering, Inorg. Chem. **24**, 2174 (1985).
[2] P. Gutlich, Y. Garcia, and T. Woike, Coord. Chem. Rev. **219**, 839 (2001).
[3] L. Wiehl, H. Spiering, P. Gütlich, and K. Knorr, J. Appl. Crystallogr. **23**, 151 (1990).
[4] L. Wiehl, Acta Crystallogr. **49**, 289 (1993).
[5] O. Kahn, *Molecular Magnetism* (VCH, New York, 1993).
[6] A. Hauser, A. Vef, and P. Adler, J. Chem. Phys. **95**, 8710 (1991).
[7] E. K. U. Gross and W. Kohn, Adv. Quantum Chem. **21**, 255 (1990).
[8] M. E. Casida, in *Recent Advances in Density Functional Methods*, edited by D. P. Chong (World Scientific, Singapore, 1995).
[9] M. E. Casida, in *Recent Developments and Applications of Modern Density Functional Theory, Theoretical and Computational Chemistry*, edited by J. M. Seminario (Elsevier, Amsterdam, 1996).
[10] C. Jamorski, M. E. Casida, and D. R. Salahub, J. Chem. Phys. **104**, 5134 (1996).
[11] W. Kohn and L. J. Sham, Phys. Rev. **140**, A1133 (1965).
[12] R. G. Parr and W. Yang, *Density-Functional Theory of Atoms and Molecules* (Clarendon, Oxford, 1989).
[13] W. Kohn, A. D. Becke, and R. G. Parr, J. Phys. Chem. **100**, 12974 (1996).
[14] J. E. Monat, J. H. Rodriguez, and J. K. McCusker, J. Phys. Chem. A **106**, 7399 (2002).
[15] E. Runge and E. K. U. Gross, Phys. Rev. Lett. **52**, 997 (1984).
[16] S. J. A. van Gisbergen, J. G. Snijders, and E. J. Baerends, Comput. Phys. Commun. **118**, 119 (1999).
[17] F. Aquino and J. H. Rodriguez, Proceedings of the Molecular Orbital Density of States Program, West Lafayette, IN, 2005 (unpublished).
[18] A. D. Becke, J. Chem. Phys. **98**, 1372 (1993).
[19] A. D. Becke, J. Chem. Phys. **98**, 5648 (1993).
[20] C. Lee, W. Yang, and R. G. Parr, Phys. Rev. B **37**, 785 (1988).
[21] A. D. Becke, Phys. Rev. A **38**, 3098 (1988).
[22] J. P. Perdew and Y. Wang, Phys. Rev. B **45**, 13244 (1992).
[23] M. J. Frisch, G. W. Trucks, H. B. Schlegel *et al.*, GAUSSIAN 98, Revision A.4, Gaussian, Inc., Pittsburgh PA, 1998.
[24] JAGUAR 4.2, Schrodinger, Inc., Portland, Oregon, 2000.
[25] G. F. Bertsch and A. Schnell, J. Chem. Phys. **115**, 4051 (2001).
[26] M. Sorai and S. Seki, J. Phys. Chem. Solids **35**, 555 (1974).
[27] Y. Ogawa, S. Koshihara, K. Koshino, T. Ogawa, C. Urano, and H. Takagi, Phys. Rev. Lett. **84**, 3181 (2000).
[28] T. Chachiyo and J. H. Rodriguez (unpublished).
[29] W. J. Hehre, R. Ditchfield, and J. A. Pople, J. Chem. Phys. **56**, 2257 (1972).